

Non-uniqueness in Inverse Problems: a Case Study

Amir H Hosseini and Clayton V Deutsch

It is well-known that inverse problems are prone to stability and non-uniqueness problems. The idea in this paper is to investigate the non-uniqueness problem arising from simultaneous estimation of mass transport parameters that are responsible for introducing and removing mass from saturated aquifers. The study is implemented using 1D and 2D examples, where bivariate relationships among the sensitivity coefficients is investigated and objective function surfaces are plotted. It is observed that designing an appropriate monitoring network and defining the weighting scheme in the objective function inverse proportional to the value of simulated concentration can effectively mitigate the non-uniqueness problem.

Introduction

Simultaneous characterization of uncertainty in rate-limited dissolution and field-scale biodegradation is important for development of an advanced screening tool for management of the TOR problems; but it is subject to potential numerical instabilities. For a real site with crude oil (BTEX) contamination and a simple representation of the source zone, Essiad et al. (2003) implemented inverse modeling in an 'optimal' sense to estimate NAPL dissolution rate and individual first-order biodegradation rates for BTEX compounds as well as other parameters such as the recharge rate, hydraulic conductivity, and transverse dispersivity. They only achieved convergence when they estimated a single dissolution rate for all BTEX compounds and coupled the simulation of BTEX compounds through simultaneous use of oxygen during aerobic biodegradation (crossover effect). In other words, they failed to estimate individual dissolution rate and first-order biodegradation constants for each BTEX component due to high correlation between these parameters that results in parameter non-uniqueness. As pointed out by Carrera and Neuman (1986) and reviewed by Friedel (2005) and Carrera et al. (2005), the four primary reasons for parameter non-uniqueness are precision of numerical solution (e.g. round-off errors in calculation of sensitivities), numerical dispersion, local minima in parameter space and correlation among parameters. In the problem of simultaneous estimation of dissolution rate and biodegradation rate, non-uniqueness (uncertainty) of the parameter estimates is not only due to above-mentioned numerical instabilities, but also due to uncertainty in model structure and/or values of other hydrogeological or mass transport parameters. The uncertainties in the values of dissolution rate and first-order biodegradation rate due to uncertainty in model structure are investigated in Hosseini and Deutsch (2009) through implementation of stochastic inverse modeling. In this paper, the existence of local minima and high correlation among model parameters are investigated in the following 1D and 2D examples.

Correlation between the parameters: 1D case

To investigate the correlations between the parameters, first, a 1D example is presented where the sensitivity of concentrations with respect to the changes in the dissolution rate and first-order biodegradation rate ($S_{k_{dis}}$ and S_{λ}) are calculated and their relationship is studied. For a one-dimensional case, the mass transport equation can be written by:

$$\frac{\partial(C_x)}{\partial t} = \frac{\partial}{\partial x} \left(D_{xx} \frac{\partial C_x}{\partial x} \right) - \frac{\partial}{\partial x} (v_x C_x) + \max[0, k_{dis} (C^{eq} - C_x)] - \lambda C_x \quad [1]$$

where, only the velocity and dispersion coefficient in the x direction have been retained and the subscript s that represents solute species has been replaced by x to show that concentration is a function of space. Also, in Equation [1], the dispersion coefficient D_{xx} can be replaced by $\alpha_L |v_x|$, where α_L is longitudinal dispersivity and v_x is the local velocity. Differentiation of Equation [1] with respect to k_{dis} and λ results in:

$$\frac{\partial S_{\lambda}}{\partial t} = \alpha_L v_x \frac{\partial^2 S_{\lambda}}{\partial x^2} + \left(\alpha_L \frac{\partial v_x}{\partial x} - v_x \right) \frac{\partial S_{\lambda}}{\partial x} - \left(k_{dis} + \lambda + \frac{\partial v_x}{\partial x} \right) S_{\lambda} - C_x \quad [2]$$

$$\frac{\partial S_{k_{dis}}}{\partial t} = \alpha_L v_x \frac{\partial^2 S_{k_{dis}}}{\partial x^2} + \left(\alpha_L \frac{\partial v_x}{\partial x} - v_x \right) \frac{\partial S_{k_{dis}}}{\partial x} - \left(k_{dis} + \lambda + \frac{\partial v_x}{\partial x} \right) S_{k_{dis}} + \max[0, k_{dis} (C^{eq} - C_x)] \quad [3]$$

where, all terms have been defined previously. Also, one can differentiate the Equation [1] with respect to the local velocity v_x . After rearranging, one can find the partial differential equation for the sensitivity of the local concentration with respect to the local velocity field (S_{v_x}):

$$\frac{\partial S_{v_x}}{\partial t} = \alpha_L v_x \frac{\partial^2 S_{v_x}}{\partial x^2} + \left(\alpha_L \frac{\partial v_x}{\partial x} - v_x \right) \frac{\partial S_{v_x}}{\partial x} - \left(k_{dis} + \lambda + \frac{\partial v_x}{\partial x} \right) S_{v_x} + \alpha_L \frac{\partial^2 C_x}{\partial x^2} - \frac{\partial C_x}{\partial x} \quad [4]$$

where, all terms have been defined previously.

Equations [2], [3] and [4] can be discretized by finite difference method and solved numerically. Figure 1 shows the reference 1D hydraulic conductivity and head distribution and the development of the 1D plume until reaching to a semi-steady-state condition. The length of the 1D simulation domain is 300m, and the reference k_{dis} and λ are 0.0015 day^{-1} and 0.0044 day^{-1} . The flow and transport boundary conditions include fixed head boundaries of 8m and 2m, and zero dispersive flux boundaries at both ends.

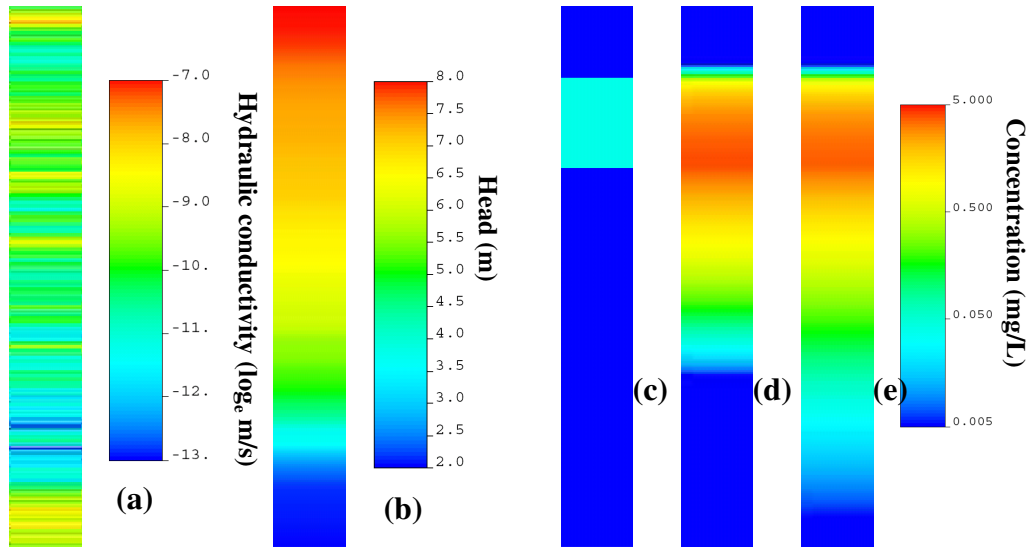


Figure 1: (a) The reference (a) transmissivity, (b) steady-state head and concentration (c) after 2 days, (d) after 732 days, and (e) after 2562 days.

Figures 2-a, b show (1) there exists a high correlation (for the given values of the parameters) between the sensitivities of the concentrations with respect to perturbations of dissolution rate and first-order biodegradation rate inside and outside of the source zone; and (2) the correlation between these parameters differs inside and outside of the source both in terms of magnitude of the sensitivities and in terms of the trends in the correlations (positive or negative). As shown in the subsequent 2D example, the observed changes in the correlations outside and inside of the source can be used to avoid instabilities in the inverse problem. In Figures 2-c, d, e, f, the cross-plots between the sensitivities of concentrations with respect to perturbations of local velocity field and the two transport parameters are presented. According to these figures, a very high correlation between these parameters is observed. Nevertheless, making any conclusive argument about requirement of decoupling the flow and transport inverse problems from this observation relies on the assumption of independency of local velocities at different locations, which is an invalid assumption. Thus, although one can not make a conclusive argument about decoupling of the inverse problems (subject to further research), the observations in Figures 2-c, d, e, and f show that when the observation locations are sparse and the range of spatial correlation of hydraulic conductivity is small, there may potentially be a high correlation between these parameters that may have an adverse effect on the stability of the coupled problem. This is subject to future research.

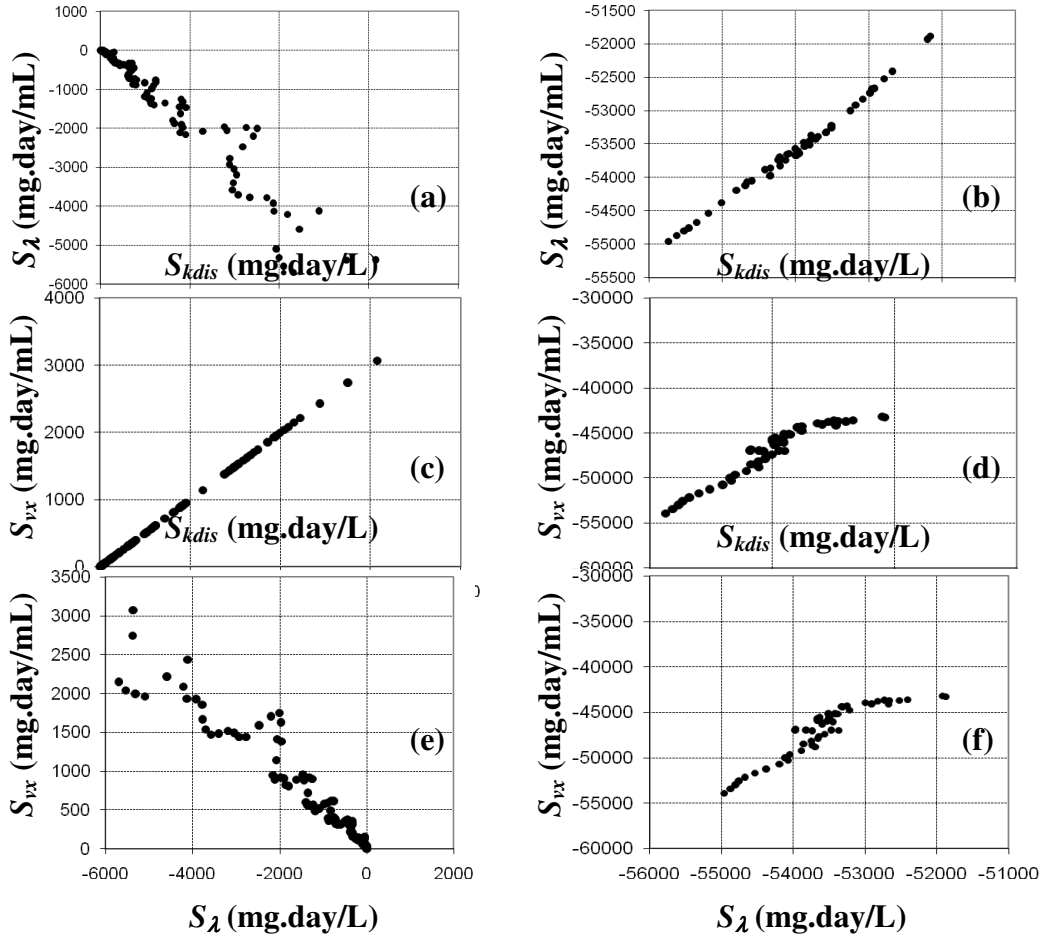


Figure 2: The cross-plots between (c) S_λ and $S_{k_{dis}}$ away from the source, (d) S_λ and $S_{k_{dis}}$ in the source zone, (c) S_{v_x} and $S_{k_{dis}}$ away from the source, (d) S_{v_x} and $S_{k_{dis}}$ in the source zone, (e) S_{v_x} and S_λ away from the source, and (f) S_{v_x} and S_λ in the source zone. The cross-plots show the correlation between the sensitivities at time step 2562 days for k_{dis} and α values equal to 0.0015 day⁻¹ and 0.0044 day⁻¹, respectively.

Correlation between the parameters: 2D case

The correlations between the parameters and existence of local minima can also be investigated in a 2D example. In 2D, the governing mass transport equation is written by:

$$\frac{\partial(\theta C_s)}{\partial t} = \frac{\partial}{\partial x_i} \left(\theta D_{ij} \frac{\partial C_s}{\partial x_j} \right) - \frac{\partial}{\partial x_i} (\theta v_i C_s) + \theta \cdot \max[0, k^{NAPL} (C_s^{eq} - C_s)] - \theta \lambda C \tag{5}$$

where, θ , k_i , h , q_{sr} , C , D_{ij} , v_i , k_{dis} , C^{eq} , and λ represent porosity, hydraulic conductivity, hydraulic head, dispersion coefficient, seepage velocity, NAPL dissolution rate constant, equilibrium concentration, and first-order biodegradation rate constant.

Figure 3 shows the synthetic study site that has a heterogeneous hydraulic conductivity with a log-normal Gaussian distribution with a mean of -10.5 (log_e m/s), standard deviation of 0.8 (log_e m/s), and a spherical variogram with a nugget equal to 0.05 and a range equal to 30m. No-flow boundary conditions are assigned at the west and the east of the site and constant head boundary conditions equal to 3.6 m and

2.0 m are assigned at the north and the south of the site, respectively. In terms of mass transport properties and boundary conditions, a rectangular NAPL source zone was considered at the north of the site with a uniform substrate (e.g. benzene) soil concentration equal to 100mg/Kg, assuming that the initial mass fraction of the substrate in the NAPL is equal to 0.01. The substrate solubility, substrate and inert molecular weights are set equal to 0.00178gr/cm³, 78.1 and 101gr/mole, respectively. Dry soil density, total porosity and effective porosity are set equal to 1.6gr/cm³, 0.35 and 0.3, respectively. The dissolution rate and first-order biodegradation rates are set equal to 0.0011day⁻¹, and 0.0044day⁻¹, respectively. Zero dispersive flux boundary conditions are assigned at all boundaries. The longitudinal and transverse dispersivities are set equal to 1.0m and 0.2m, respectively. Figure 4 shows a few snap-shots of the development of the plume, which has been simulated for 10 years.

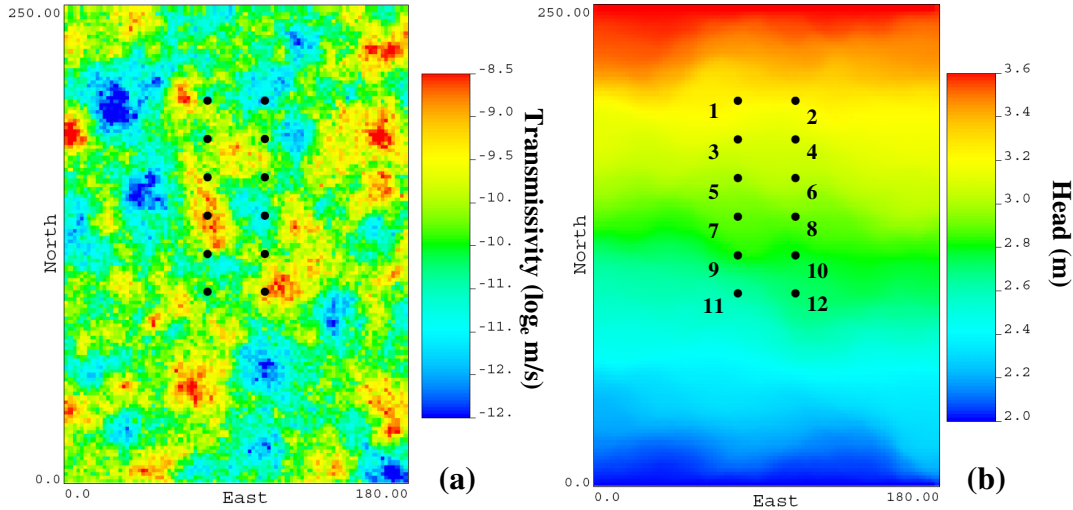
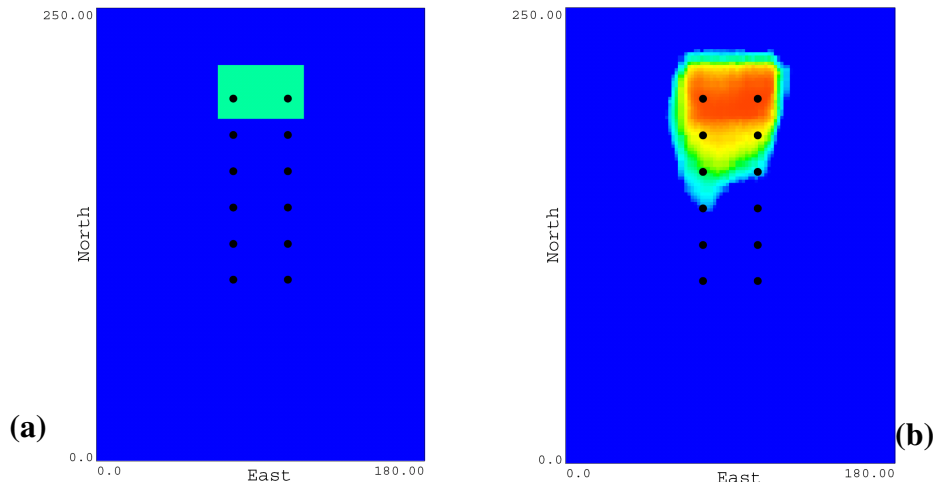


Figure 3: (a) Reference hydraulic conductivity field, and (b) the associated piezometric head response. The monitoring locations numbered 1 to 12 are used to record the simulated concentrations and plot the objective function surface in Section 5.2.3.

Figure 5 shows the cross-plots between the values of the $S_{k_{dis}}$ (always positive) and the absolute values of S_{λ} (always negative) in the 2D example for different values of dissolution rate. In the cross-plots shown in Figure 5, the location of the calculated sensitivity coefficients is highlighted using a gray-scale color bar, where the black end represents the points closer to the source zone, and light-grey end represents the points more away from the source zone.



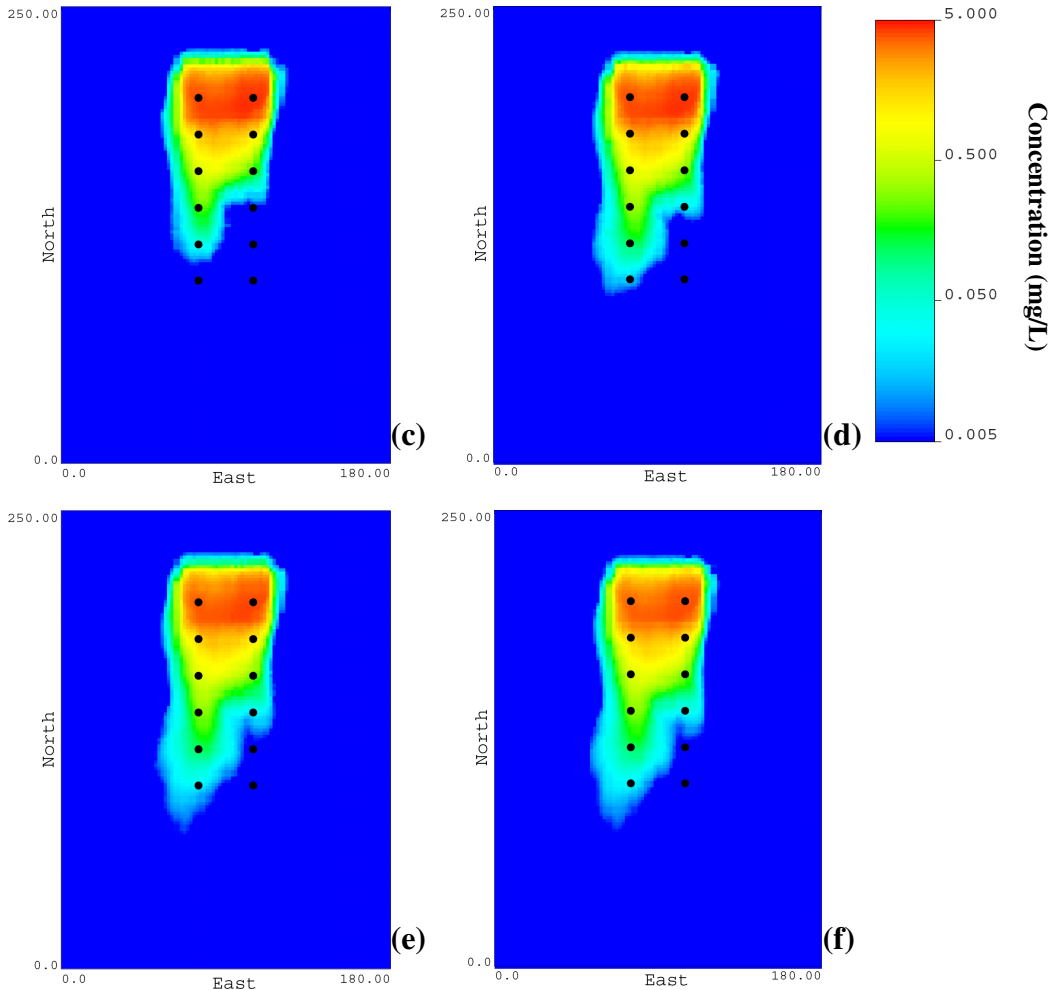


Figure 4: Six snapshots from the development of the dissolved contaminant plume after (a) 1 day, (b) 1 year, (c) 2 years, (d) 3 years (e) 7.5 years and (f) 10 years.

Similar to what observed for the 1D case, Figure 5 shows the value of $S_{k_{dis}}$ strongly depends on the value of the dissolution rate, and as the value of dissolution rate becomes smaller, larger correlation is observed between the sensitivity coefficients inside and outside of the source. Both $S_{k_{dis}}$ and S_{λ} sensitivities are also variable in time. The most important observations and conclusions related to Figures 5 are: (1) for large values of the dissolution rate, the correlation between the two parameters becomes smaller and parameter non-uniqueness becomes less of an issue. For this case, however, parameter insensitivity may become the problem; (2) for smaller values of dissolution rate (which are more feasible for real field applications according to Essaid et al. (2003) and Christ et al. 2006), a very high correlation exists between the two sensitivities. It is also observed that there are two different correlations between the two parameters depending on the location of the calculated sensitivities (similar to the 1D case). The fact that there exist two different correlations can be used together with definition of weights inverse proportional to the simulated concentration to improve the stability of the inverse problem. This can be achieved through designing the monitoring network in such a way that observation locations sample the locations close to the source zone as well as the locations well-away from the source, while the weighting scheme in the objective function has to be defined by:

$$F'_{C,j} = \sum_{i=1}^{n_c} q_j w_i (C_i^m - C_i)^2 \quad \text{with} \quad w_i = \frac{1}{cv_i^2 C_i^2} \quad [6]$$

where, C_i , C_i^m , q_i and cv_i are simulated concentration, measured concentration, source size quantile and coefficient of variation associated with each observation. If one also includes prior information for parameter values, the objective function will be:

$$F_{C,j} = q_j \sum_{i=1}^{n_c} w_i (C_i^m - C_i)^2 + w_k (\ln k_{dis}^{PR} - \ln k_{dis})^2 + w_\lambda (\ln \lambda^{PR} - \ln \lambda)^2 \quad [7]$$

where, k_{dis}^{PR} , k_{dis} , λ^{PR} and λ represent the prior value for the dissolution rate, the estimated value for the dissolution rate, the prior value for first-order biodegradation rate, and the estimated value for first-order biodegradation rate, respectively. The weights w_k and w_λ are calculated as the inverse of the variance of the prior values:

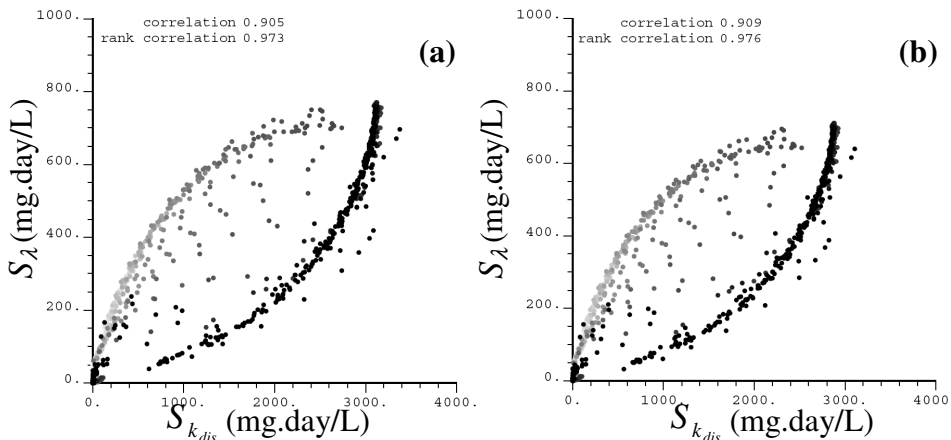
$$w_k = \frac{1}{\sigma_{\ln k}^2} \quad \text{and} \quad w_\lambda = \frac{1}{\sigma_{\ln \lambda}^2} \quad [8]$$

where, $\sigma_{\ln k}$ and $\sigma_{\ln \lambda}$ are the standard deviations of prior values for dissolution rate and first-order biodegradation rate, respectively. The gradient of the objective function (Equation [7]) with respect to the transport parameters is calculated by:

$$\frac{\partial F_{C,j}}{\partial \alpha} = q_j \sum_{i=1}^{ND} \left[\frac{2C_i^m}{cv_i^2 C_i^2} \left(1 - \frac{C_i^m}{C_i} \right) S_{\alpha,i} \alpha \right] + \frac{2}{\sigma_{\ln k}^2} \alpha (\ln \alpha - \ln \alpha^m) \quad \text{with} \quad \alpha = k_{dis}, \lambda \quad [9]$$

that ensures preservation of sensitivity of the objective function with respect to sensitivity of the concentration with changes in the parameter values.

The fact that designing an appropriate layout for the monitoring network improves the stability of the inverse problem for small values of dissolution rate can also be investigated through plotting the objective function surfaces (Figures 6, 7 and 8). The synthetic aquifer shown in Figure 5-6 with 12 monitoring locations is used for this purpose. The monitoring data sampled from the synthetic plume are recorded when the plume is under a steady-state condition at the time steps of 8 years, 8.5 years, 9 years, 9.5 years and 10 years. As shown in Figures 6 to 8, the objective function surfaces have been plotted with and without prior information, using the equations [5.16] and [5.15], respectively. The true parameter values used to create the reference case include $k_{dis} = 0.0011 \text{ day}^{-1}$ and $\lambda = 0.0044 \text{ day}^{-1}$. The prior information are included in calculation of the objective function using Equations [5.16] and [5.17]; and they are considered to have log-normal distributions with a mean (k_{dis}^{PR}) of 0.001 day^{-1} and standard deviation ($\sigma_{\ln k}$) of $1.0 \log_e \text{day}^{-1}$ for the dissolution rate and a mean (λ^{PR}) of 0.0045 day^{-1} and standard deviation ($\sigma_{\ln \lambda}$) of $0.3 \log_e \text{day}^{-1}$ for the first-order biodegradation rate.



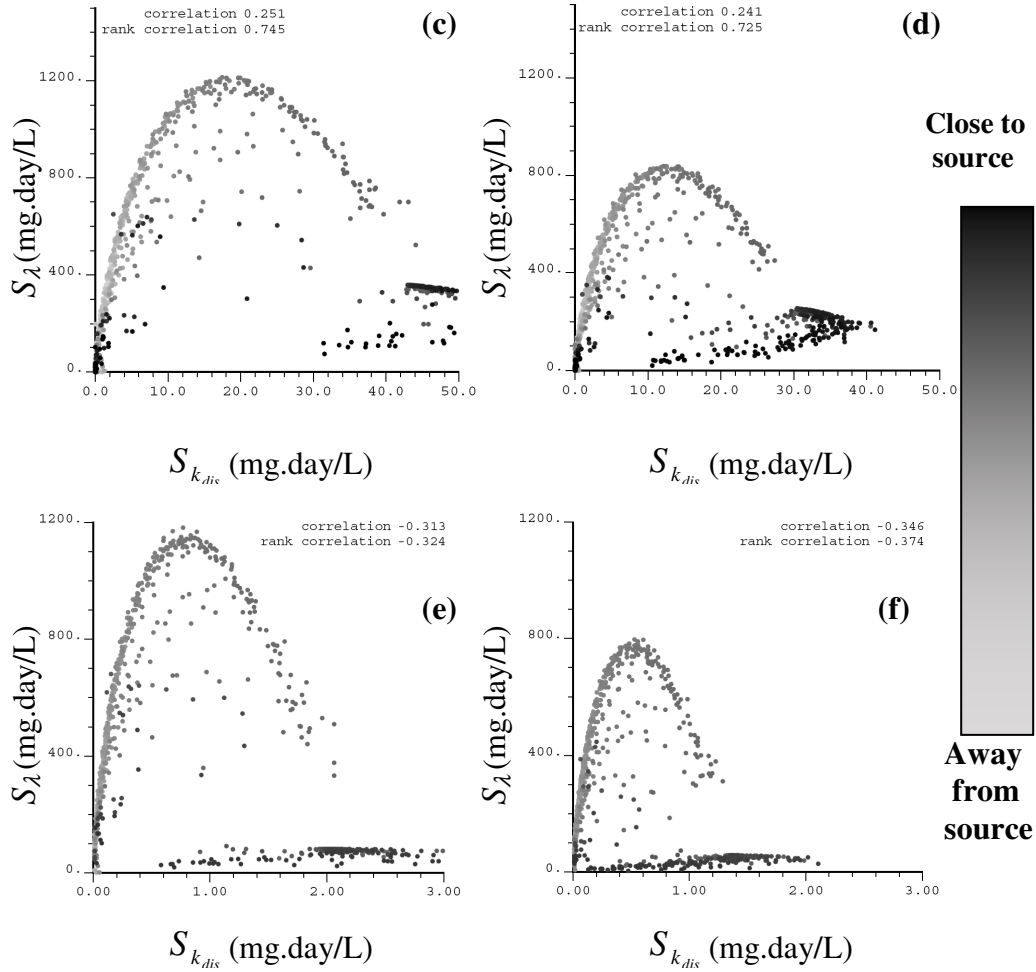


Figure 5: The cross-plots between the values of $S_{k_{dis}}$ and the absolute values of S_{λ} for (a) $k_{dis}=0.0011\text{day}^{-1}$ and $T=5\text{yrs}$, (b) $k_{dis}=0.0011\text{day}^{-1}$ and $T=10\text{yrs}$, (c) $k_{dis}=0.011\text{day}^{-1}$ and $T=5\text{yrs}$, (d) $k_{dis}=0.011\text{day}^{-1}$ and $T=10\text{yrs}$, (e) $k_{dis}=0.175\text{day}^{-1}$ and $T=5\text{yrs}$, (f) $k_{dis}=0.175\text{day}^{-1}$ and $T=10\text{yrs}$. The gray-scale color bar shows the location of the calculated sensitivity coefficients.

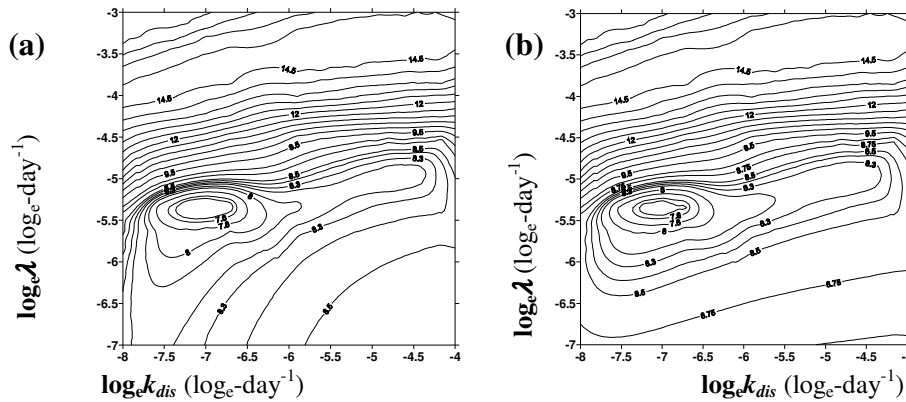


Figure 6: The objective function surfaces plotted based on observations in wells 1 to 12, (a) without any prior information and (b) with prior information.

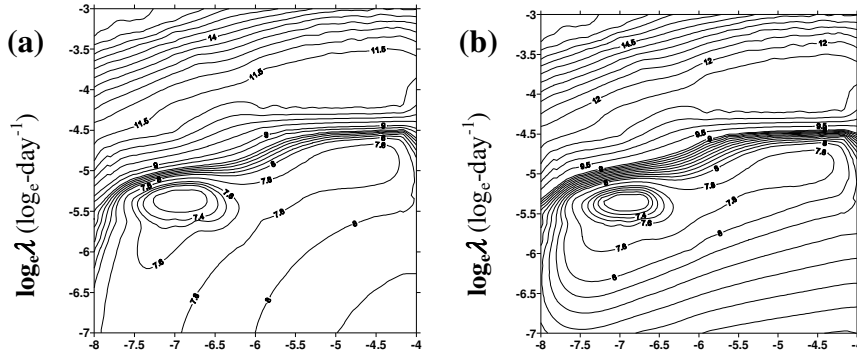


Figure 7: The objective function surfaces plotted based on observations in wells 1 to 4, and 9 to 12 (a) without any prior information and (b) with prior information.

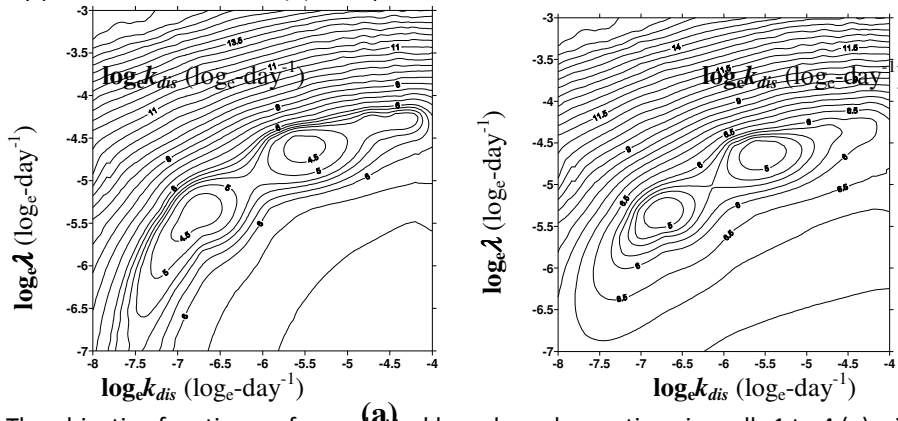


Figure 8: The objective function surfaces plotted based on observations in wells 1 to 4 (a) without any prior information and (b) with prior information.

In Figure 6, monitoring data includes samples from all 12 wells. In Figure 7 monitoring data includes samples from wells 1 to 4 at the upstream of the site and wells 9 to 12 at the downstream of the site; and in Figure 8 monitoring data includes samples from wells 1 to 4 at the upstream of the site (in the source and close to the source zone). It is evident from the Figures 6 to 8 that if the layout for the monitoring network is designed in such a way that the upstream (near the source zone) as well as downstream (near the edge of the plume) are sampled, the stability of the problem will significantly be improved. Comparing Figures 6 and 7, one may also observe that inclusion of the middle wells in calculation of the objective function has little effect on the improvement of the stability of the problem. The prior information has a secondary effect on the stability of the inverse problem. Although a good set of priori information are used to create the objective function surface in Figure 8-b, it has not avoided the problem of a local minima in this case. Comparing Figure 6-b to Figure 6-a and Figure 7-b to Figure 7-a, one can observe that inclusion of good prior information only slightly improves the stability of the problem.

References

Carrera, J. and S.P. Neuman (1986) Estimation of aquifer parameters under transient and steady-state condition. 1. Maximum likelihood method incorporating prior information, *Water Resources Research*, 22(2), 199-210
 Carrera, J., A. Alcolea, A. Medina, J. Hidalgo, and L.J. Slooten (2005), Inverse problem in hydrogeology, *Hydrogeology Journal*, 13(1), 206-222
 Christ, J.A., C.A. Ramsburg, K.D. Pennell, and L.M. Abriola (2006) Estimating mass transfer from dense nonaqueous phase liquid source zones using upscaled mass transfer coefficients: An evaluation using multiphase numerical simulations, *Water Resources Research*, 42(11), W11420
 Essaid, H.I., I.M. Cozzarelli, R.P. Eganhouse, W.N., Herkelrath, BA. Bekins, G.N. Delin (2003), Inverse modeling of BTEX dissolution and biodegradation at the Bemidji, MN crude-oil spill site, *Journal of Contaminant Hydrology*, 67(1-4), 269-299
 Friedel, M.J. (2005), Coupled inverse modeling of vadose zone water, heat, and solute transport: calibration constraints, parameter nonuniqueness, and predictive uncertainty, *Journal of Hydrology*, 312, 148-175
 Hosseini, A.H., C.V. Deutsch (2009), Stochastic inverse modeling in a mass transport problem, *Center for Computational Geostatistics, Report 11*, paper 115